

## INFRARED SPECTRA OF SILICA POLYMORPHS AND THE CONDITIONS OF THEIR FORMATION

C. KOIKE<sup>1</sup>, R. NOGUCHI<sup>2</sup>, H. CHIHARA<sup>3,5</sup>, H. SUTO<sup>4</sup>, O. OHTAKA<sup>2</sup>, Y. IMAI<sup>2</sup>, T. MATSUMOTO<sup>2</sup>, AND A. TSUCHIYAMA<sup>3</sup>

<sup>1</sup> Department of Physics, Ritsumeikan University, Kusatsu, Shiga 525-8577, Japan; [koike-c@mua.biglobe.ne.jp](mailto:koike-c@mua.biglobe.ne.jp)

<sup>2</sup> Department of Earth and Space Science, Graduate School of Science, Osaka University, Toyonaka, Osaka 560-0043, Japan

<sup>3</sup> Division of Earth and Planetary Sciences, Graduate School of Science, Kyoto University, Kitashirakawa, Sakyo, Kyoto 606-8052, Japan

<sup>4</sup> National Astronomical Observatory of Japan, Mitaka, Tokyo 181-8588, Japan

Received 2012 November 19; accepted 2013 September 9; published 2013 November 6

### ABSTRACT

The existence of silica within several debris disks has been suggested. Data on both the spectroscopy and annealing conditions of the various polymorphs of silica need to be investigated, as these data are lacking and incomplete in the literature. We investigate the annealing conditions of silica and prepare various types of silica, including  $\alpha$ -cristobalite,  $\alpha$ -quartz, coesite, stishovite, and fused quartz, which are natural, synthetic, or commercial samples. This paper presents a new study of both the spectroscopy of relevant silica polymorphs and the conditions under which they form. We compare the results to previous studies and find that there are discrepancies. The interesting result of features similar to those of forsterite should be highlighted, where  $\alpha$ -cristobalite and coesite showed similar peaks at 16, 33, and 69  $\mu\text{m}$  as forsterite. The 69  $\mu\text{m}$  band for  $\alpha$ -cristobalite is especially very broad and strong and shifts largely to a shorter wavelengths under cooling to low temperatures. The band for coesite, however, is very sharp and shifts only a small amount to longer wavelengths under cooling to low temperatures. We discuss the possibility of silica detection around debris disks.

**Key words:** circumstellar matter – infrared: planetary systems – methods: laboratory: solid state – stars: individual (HD 15407)

*Online-only material:* color figures

### 1. INTRODUCTION

Recently, certain unusual features were detected in debris disks HD 172555, HD 15407A, HD 23514A, and HD 23514, in which prominent peaks appeared at about 9.3, 12, and 21  $\mu\text{m}$  (Lisse et al. 2009) and at about 9, 16 and 20–22  $\mu\text{m}$  (Melis et al. 2010; Rhee et al. 2008; Fujiwara et al. 2012b). The unusual spectra of HD 15407 observed by Fujiwara et al. (2012b) were particularly notable, as two significant emission peaks occurred at about 9 and 20  $\mu\text{m}$ , and a weak peak at 16  $\mu\text{m}$  was also detected. The spectra fit well with amorphous silicate (amorphous pyroxene), fused silica, and annealed silica. The annealed silica explains the feature observed at 16  $\mu\text{m}$ , while producing a sharp extra emission at 12.6  $\mu\text{m}$  (Fujiwara et al. 2012b). Olofsson et al. (2012) reported similar results, according to which a significant fraction of  $\text{SiO}_2$  (annealed silica as cristobalite) is required, fitting the observed spectrum of HD 15407. Within our solar system, silica is one of the most abundant minerals in the Earth’s crust. However, it is not observed in the interstellar medium toward the galactic center, since the expected bands at about 9 and 12.6  $\mu\text{m}$  are not detected (Kemper et al. 2004). Around the circumstellar regions of young and evolved stars, sharp peaks due to Mg-rich crystalline silicates have been detected in the wide-wavelength regions (Malfait et al. 1998; Molster et al. 2002). Many O-rich asymptotic giant branch stars exhibit the spectra at about 10  $\mu\text{m}$  and 13  $\mu\text{m}$ , where there is a close correlation of the strength of the 13  $\mu\text{m}$  band with that of the 10  $\mu\text{m}$  silicate band, and the silicates could be promising candidates (Begemann et al. 1997; Speck et al. 2000). Speck et al. (2000) suggested the 13  $\mu\text{m}$  feature could be associated with  $\text{SiO}_2$  or highly polymerized silicates (not pyroxenes or olivines). Afterward, grains definitely containing silica minerals were positively

suggested in explaining the spectra of the T Tauri star (TTS) HEN 3-600A, which shows multiple local peaks at 9.2, 10.1, 10.5, 10.9, 11.2, and 12.5  $\mu\text{m}$ . In this case, silica in the form of quartz is used to explain the peak positions at 9.2 and 12.5  $\mu\text{m}$  (Honda et al. 2003). Watson et al. (2009) also detected  $\alpha$ -quartz features at about 9 and 12.5  $\mu\text{m}$  in the *Spitzer*-Infrared Spectrograph (IRS) spectrum of IS Tau. HD 172555 exhibits infrared (IR) spectra at approximately 9.3 and 19  $\mu\text{m}$  with subtle peaks at 7.5–8.2, 11.2, and 33  $\mu\text{m}$ ; the spectra of silicates such as obsidian and tektite fit the observed data well (Lisse et al. 2009). Furthermore, several TTSs show prominent narrow emission features indicating annealed silica, where two polymorphs of silica, tridymite and cristobalite, are dominant (Sargent et al. 2009). Annealed silica was first suggested as a component of circumstellar TTS dust, which is synthesized after the annealing of fused quartz at 1220 K for 4.5–5 hr (Fabian et al. 2000). Furthermore, coesite and stishovite were discovered in lunar meteorite Asuka-881757 (Ohtani et al. 2011). Coesite was also discovered in carbonaceous chondrites (Gujba chondrites; Weisberg et al. 2006). These high-pressure polymorphs of  $\text{SiO}_2$  indicate that the meteorite experienced a minimum equilibrium shock pressure of 8–30 GPa. As for the debris disk, it is widely accepted that terrestrial planet building may be still progressing through large, violent collisions that could yield large amounts of debris and significant IR excesses (Meng et al. 2012; Fujiwara et al. 2012b). The presence of strong features at 8–9  $\mu\text{m}$  by silica dust and SiO gas toward HD 172555 could be explained by large hypervelocity ( $>10 \text{ km s}^{-1}$ ) impacts giving rise to high-temperature processes between large rocky planetesimals, which occur in events similar to the lunar formation event between large differentiated planetesimals (Lisse et al. 2009). Therefore, evidence of high-pressure impact metamorphism and the formation of high-pressure minerals such as coesite and stishovite may be observed in debris disks.

The term “silica,” which technically refers to silicon dioxide ( $\text{SiO}_2$ ), is used erroneously in solid state, astronomy, and other

<sup>5</sup> Currently at College of General Education, Osaka Sangyo University, Daito, Osaka 574-8530, Japan.

**Table 1**  
Silica (SiO<sub>2</sub>) Polymorphs at Low and High Pressures

(1) Low-pressure Silica Polymorphs (For pressures of 1 atom or lower)			
$\beta$ -Quartz (Hexagonal) 846 K–1143 K stable	$\beta$ -Tridymite (Hexagonal) 1143 K–1743 K stable 390 K–1143 K metastable	$\beta$ -Cristobalite (Cubic) >1743 K stable 543 K–1743 K metastable	Silica Glass (Amorphous) $\leq 1300$ K
	$\updownarrow$	$\updownarrow$	*Common name Amorphous silica, Fused quartz, Vitreous silica, Silica glass, Quartz glass, Fused silica, Synthetic fused silica,
$\alpha$ -Quartz (Trigonal) <846 K stable	$\alpha$ -Tridymite (Orthorhombic) <390 K metastable	$\alpha$ -Cristobalite (Tetragonal) <543 K metastable	
(2) High-pressure Silica Polymorphs (At higher pressures ( $P$ ) and a wide range of temperatures ( $T$ ))			
Coesite $2 \text{ GPa} < P < 11 \text{ GPa}$ (Monoclinic, tetrahedral coordination)	800 K < $T$ < 3000 K stable		
Stishovite $P > 8 \text{ GPa}$ (Octahedral (six-fold) coordination, Rutil structure)	800 K < $T$ < 3300 K stable		

**Note.** Details in the text. ( $\updownarrow$ ): means crystal system.

fields to describe products such as quartz, vitreous silica, and cristobalite. In particular, astronomers have used the term to describe quartz in some cases and annealed silica in others.

Silicon dioxide SiO<sub>2</sub> can exist as either crystalline or amorphous. The basic structural unit of crystalline silica is the tetrahedron with the oxygen atoms at the corners and the silicon atom in the center. According to the phase diagram of silica (Deer et al. 1999; Klein & Hurlbut 1993; Swamy & Saxena 1994; Speck 1998) and online at The Quartz Page ([http://www.quartzpage.de/gen\\_mod.html](http://www.quartzpage.de/gen_mod.html) and [http://serc.carleton.edu/research\\_education/equilibria/metamorphic\\_diagrams.html](http://serc.carleton.edu/research_education/equilibria/metamorphic_diagrams.html)), low-pressure silica polymorphs and high-pressure silica polymorphs are formed as shown in Table 1 and Figure 1. There are three main low-pressure forms or polymorphs of crystalline SiO<sub>2</sub>: quartz, tridymite, and cristobalite. These forms are metastable outside the temperature range of formation, and each are split into two types,  $\alpha$  and  $\beta$ , according to the temperature of formation. If cooling is rapid enough to prevent crystallization below glass transition temperature ( $T_g$ ), the structure will form as silica glass SiO<sub>2</sub> (Speck et al. 2011). In this case, silica glass is called by one of its common names, such as amorphous silica, fused quartz, vitreous silica, silica glass, quartz glass, fused silica, and synthetic fused silica.<sup>6</sup>

The high-pressure silica polymorphs, coesite and stishovite, form at higher pressures and a wide range of temperatures (Swamy & Saxena 1994). Each of the crystalline forms of silica have a different crystal system, such as trigonal, hexagonal, orthorhombic, hexagonal, tetragonal, cubic, monoclinic, and octahedral (six-fold) coordination, as shown in Table 1. We can estimate the formation conditions (temperature and pressure) of the silica dust in astronomical environments based on the polymorphs of silica that can be inferred from their IR spectra. As Speck et al. (2011) noted about grain structure and phase in astrophysical environments, it is important to have tools

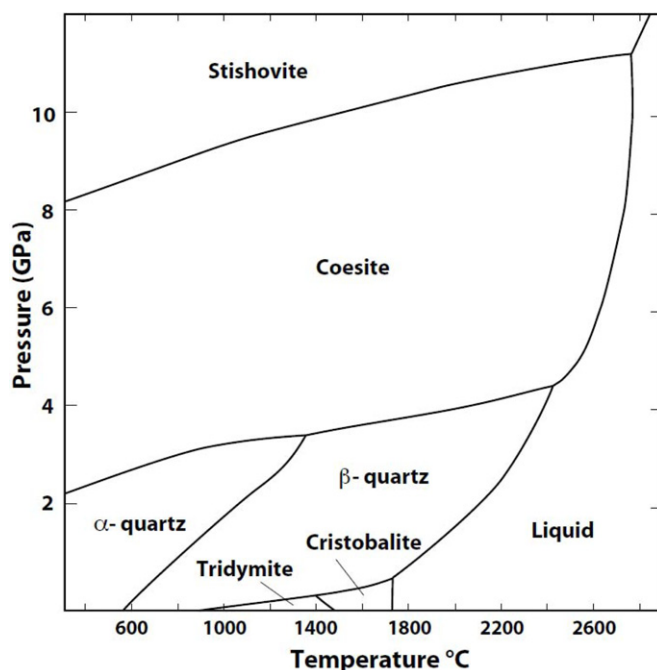


**Figure 1.** Phase diagram of silica based on Swamy & Saxena (1994). This diagram can be found at [http://serc.carleton.edu/research\\_education/equilibria/metamorphic\\_diagrams.html](http://serc.carleton.edu/research_education/equilibria/metamorphic_diagrams.html).

to distinguish whether a solid is glassy, crystalline, or some combination of the two; this has implications for its formation, and subsequent processing, evolution, and destruction. That is, the amorphous silicate spectra and their variations in strength, width, and peak position potentially provide the diagnostic tools to understand the detailed mechanisms by which dust is formed, processed, and destroyed. However, the laboratory data that exists in the literature covers neither a broad enough spectral range nor enough silica polytypes to achieve this goal. In this study, we measured the IR spectra of the various silica polymorphs over a broad range of wavelengths, i.e., in mid- and

<sup>6</sup> Possible grain types were described in detail by Speck et al. (2011), where the difference between glasses and crystals, including structural disorder and porosity, and simple phase diagram illustration of the glass transition ranging below the melting point of crystalline materials were well described.

**Table 2**  
Present and Previous Experiments Creating  $\alpha$ -Cristobalite by Annealing Amorphous Silica

Sample Preparation		$T$ (K)	Duration (hr)	Results
Annealing in lab	Fused quartz powder	1073	1	no
		1273	1, 5, 7	no
		1373	48	no
		1423	96, 192	no
		1473	1	no
		1473	72	subtle
		1773	72, 144	cr
Commercial cristobalite	Omura Ceratec Inc., Japan			
Šimon & McMahon (1953)	Glass layer	1673	No data	cr
Plendl et al. (1967)	Fused quartz plate (0.4 mm)	1725	16	cr
Bates (1972)	Glass slab (2 mm)	1813	17	cr
Ocaña et al. (1987)	Powder	1753	8	cr
Yahagi et al. (1994)	Powder	1773	2	cr
Finnie et al. (1994)	Silica glass	1873	48	cr
Fabian et al. (2000)	Powder	1220	4.5–5	cr, tr
Swainson et al. (2003)	Silica glass	1773	72	cr

**Notes.** no: no change in IR spectra; subtle: slight change in IR spectra; cr: cristobalite; tr: tridymite.

far-wavelength regions. Following a description of our results for the various silica polymorphs as compared with previous studies, we discuss the possibility of silica detection around debris disks.

## 2. PREPARATION AND MEASUREMENT OF SAMPLES

We prepared many types of silica polymorphs including  $\alpha$ -cristobalite, fused quartz,  $\alpha$ -quartz, coesite, and stishovite, obtained both in the laboratory and from commercial and natural samples. In this section, we describe their characteristics and preparation methods.

### 1. $\alpha$ -Cristobalite

In the laboratory, a fine powder of  $\alpha$ -cristobalite was prepared by annealing commercial fused quartz. Fine powder of fused quartz was then annealed at 1073–1473 K for various time durations and at 1773 K for 3 and 6 days and confirmed through X-ray diffraction (XRD), as shown in Table 2. A commercial sample of finely powdered  $\alpha$ -cristobalite was obtained from Omura Ceratec Inc., Japan. Natural cristobalite was obtained from Cougar, Siskiyou Co., California, USA.

### 2. Fused quartz

Commercial fused quartz was obtained from Nippon Aerosil Co., Ltd (details in Koike & Shibai 1994).

### 3. $\alpha$ -Quartz

Natural quartz (collection area unknown) was crushed by hand and further ground by a ball mill.

### 4. Coesite

Approximately 40 mg of a fine fused quartz powder enclosed in a Pt capsule was compressed at 6 GPa and 1573 K for 30 min with a cubic type multi-anvil high-pressure apparatus at Osaka University. The compressed powder became coesite, which was confirmed through XRD.

### 5. Stishovite

Approximately 25 mg and 20 mg of fused quartz fine powder, enclosed in separate Pt capsules, were pressed at 12 GPa and 1473 K for 1 hr by a Kawai-type multi-anvil high-pressure apparatus at the Institute for Study of the Earth's Interior, Okayama University, to make a stishovite, which was confirmed with XRD. The 25 mg sample

was recovered and confirmed, and the 20 mg sample was also recovered but was contaminated with agate and alumina mortars. As a result of these contaminations, the hardness<sup>7</sup> of the stishovite was very high at approximately 9.5 (Technical Reformance Specs 2012; Luo et al. 2007; Nishiyama et al. 2012).

The fine particles of the silica samples were well dispersed in KBr and polyethylene (PE) powder and were pressed, respectively, into KBr pellets and PE sheets, whose transmittance was measured with a Nicolet 670 and/or 6700 in the mid- and far-IR regions. The mass absorption coefficient  $\kappa$  was derived from the transmittance  $T$  by

$$\kappa = \frac{S}{M} \ln \frac{1}{T}, \quad (1)$$

where  $S$  is the surface area of pellets or sheets, and  $M$  is the mass of the sample particles in the pellets or sheets.

## 3. RESULTS AND DISCUSSION

### 3.1. $\alpha$ -Cristobalite

According to the results of Fabian et al. (2000), where cristobalite and tridymite appeared after annealing commercial fused quartz with diameters of 10–50 nm at 1220 K (947°C) for 4.5–5 hr, we annealed the powder of fused quartz with an average size of approximately 40 nm at 1073, 1273, and 1473 K for 1 hr. However, these samples showed no change in IR spectra from the starting spectra, as shown in Table 2. Even after annealing at high temperatures and for long durations—1273 K for 7 hr, 1373 K for 48 hr, and 1423 K for 4 and 8 days—and in addition to being quickly or slowly cooled, the IR spectra of the fused quartz did not change. However, a small quantity of cristobalite was ascertained by XRD. These results are inconsistent with those of Fabian et al. (2000), in which fused silica powder

<sup>7</sup> Here, hardness is a measure of a mineral's resistance to abrasion or scratching. This property is easily determined and is used widely for field identification of minerals. The relative hardness of minerals is determined according to the Mohs scale of hardness. In the Mohs scale, 10 common minerals are arranged in order of increasing hardness and are assigned numbers. This scale starts with 1 for the softest minerals, such as talc, and goes all the way up to 10 for the hardest minerals, such as diamond.

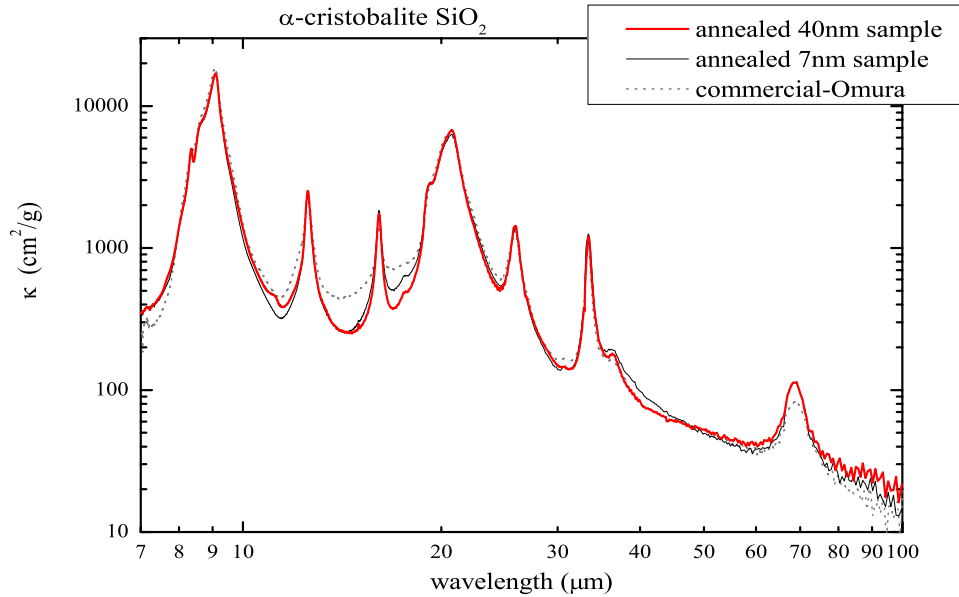


**Figure 2.** IR spectra of  $\alpha$ -cristobalite after annealed 40 nm and 7 nm samples of fused quartz at 1773 K for 3 and 6 days, respectively. The spectra for each are indicated by the thick red and thin black lines, respectively. Commercially obtained  $\alpha$ -cristobalite is represented by the dotted line.

(A color version of this figure is available in the online journal.)

was annealed at 1220 K for 4.5–5 hr and was changed into cristobalite and tridymite, confirmed by both IR spectroscopy and XRD. According to the literature, cristobalite appeared at an annealing temperature above 1673 K (Šimon & McMahon 1953; Plendl et al. 1967; Bates 1972; Ocaña et al. 1987; Yahagi et al. 1994; Finnie et al. 1994; Swainson et al. 2003) in the solid state, as indicated in Table 2, as well as in the phase diagram of silica (Figure 1, and Table 1). From the phase diagram of silica (Figure 1), we realize that the results of Fabian et al. (2000) are unusual. This result may have been due to some impurity effects or other unique conditions. Speck et al. (2011) measured the glass transition temperature of Heralsil (a very slightly hydrated silica glass) and found it to be 1420 K. This result showed the discrepancy between the present annealing results and those of Fabian. The glass transition temperatures supplied evidence that we do not expect to get annealing at such low temperatures as found by Fabian et al. (2000).

Crystallization experiments of relatively silica-rich amorphous silicates also showed that cristobalite crystallizes only at high temperatures (above 1500 K; Matsuno et al. 2012). After annealing at 1473 K for 72 hr, the IR spectra changed slightly, and small, subtle peaks appeared at 16  $\mu\text{m}$  and 33  $\mu\text{m}$ . After annealing fused quartz at 1773 K for 3 days (approximately 40 nm average size; hereafter referred to as the 40 nm sample) and 6 days (approximately 7 nm average size; hereafter called the 7 nm sample) and then rapidly cooling the samples,  $\alpha$ -cristobalite was confirmed with XRD, and the IR spectra were measured. The IR spectra of annealed silica for the 7 nm and 40 nm fused quartz samples at 1773 K were nearly same as those of commercial  $\alpha$ -cristobalite from Omura Ceratec Inc., as shown in Figure 2. Natural cristobalite showed unusual spectra because of some mineral contamination. The peaks of these cristobalite samples appeared at 8.35, 9.09, 12.5, 16.1, 20.7, 25.9, 33.5, 36.3, and 69.1  $\mu\text{m}$  and differed slightly among the samples. These spectra are similar to those of the annealed silica reported by Fabian et al. (2000); however, some peaks were shifted and others appeared due to inclusions of tridymite in their annealed silica. The peak of the 68  $\mu\text{m}$  band was shifted approximately 1  $\mu\text{m}$  longer than that recorded in our data.

Here after, the IR spectra of  $\alpha$ -cristobalite shown are from the 40 nm fused quartz sample annealed at 1773 K for 3 days. The IR spectra of  $\alpha$ -cristobalite showed several prominent peaks, as indicated in Figure 2, and one part of the spectra showed peaks similar to those of forsterite at 16, 33, and 69  $\mu\text{m}$ . Forsterite ( $\text{Mg}_2\text{SiO}_4$ ) is a significant component of circumstellar dust, with prominent peaks observed at 11.2, 16, 33, and 69  $\mu\text{m}$  (Koike et al. 2006). The  $\alpha$ -cristobalite also shows characteristic peaks similar to forsterite. Its 69  $\mu\text{m}$  band was broader than that of forsterite. However, the 33  $\mu\text{m}$  band of  $\alpha$ -cristobalite appeared very sharp compared with the 33  $\mu\text{m}$  band of forsterite. The peak position of the 16  $\mu\text{m}$  band of  $\alpha$ -cristobalite was slightly shorter than that of forsterite.

The spectra of  $\alpha$ -cristobalite have been measured by many researchers, including Finnie et al. (1994), Zhang & Scott (2007), and Swainson et al. (2003). The present spectra are similar to those reported by Swainson et al. (2003) and Zhang & Scott (2007), where characteristic sharp peaks were detected at 16.0, 26.3, 33.3, and 69  $\mu\text{m}$ , and these peaks disappeared above 540 K. Bands at approximately 9.1 and 12.5  $\mu\text{m}$  became broad above 540 K; that is, phase transition occurred, and  $\alpha$ -cristobalite (tetragonal) altered to  $\beta$ -cristobalite (cubic; Finnie et al. 1994; Swainson et al. 2003; Zhang & Scott 2007), as shown in Table 1 and Figure 1.

### 3.2. Fused Quartz and $\alpha$ -Quartz

The spectra of fused quartz (40 nm sample; Koike & Shibai 1994) are shown in Figure 3. Three broad peaks appeared at 8.93, 12.3, and 20.8  $\mu\text{m}$ .

The spectra of quartz ( $\alpha$ -quartz) grains show sharp peaks at approximately 7.14, 8.56, 9.15, 12.5, 12.8, 14.4, 19.4, 21.5, 25.2, 26.9, and 37.9  $\mu\text{m}$  and a weak peak at 78.3  $\mu\text{m}$  (Figure 3). We also measured the reflectance of bulk samples (synthetic quartz sample) for the ordinary ray ( $E \perp C$ ) and extraordinary ray ( $E \parallel C$ ) with Fourier Transform (FT)/IR Nicolet 670 and/or 6700 in the wavelengths 5 and 100  $\mu\text{m}$ . The measured reflectance spectra were much the same and looked like those reported by Spitzer & Kleinman (1961). There are, however, small differences where the reflectances of the present data

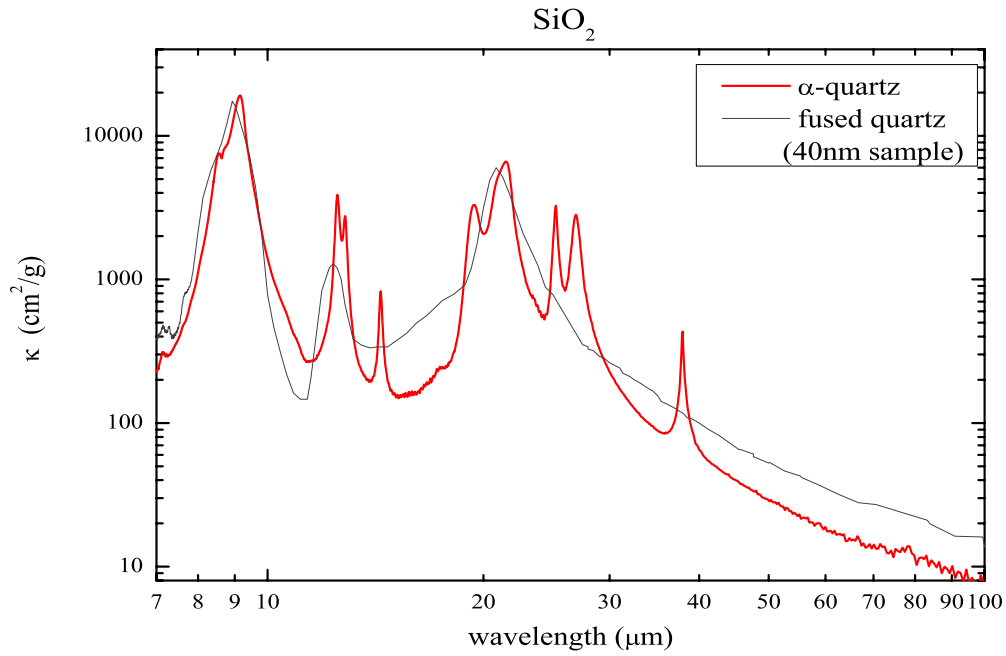


**Figure 3.** IR spectra of  $\alpha$ -quartz and fused quartz (40 nm sample) are indicated by the thick red and thin black lines, respectively. The weak peak at  $78.3 \mu\text{m}$  is consistent with the bulk data at  $78.12 \mu\text{m}$  reported by Russell & Bell (1967).

(A color version of this figure is available in the online journal.)

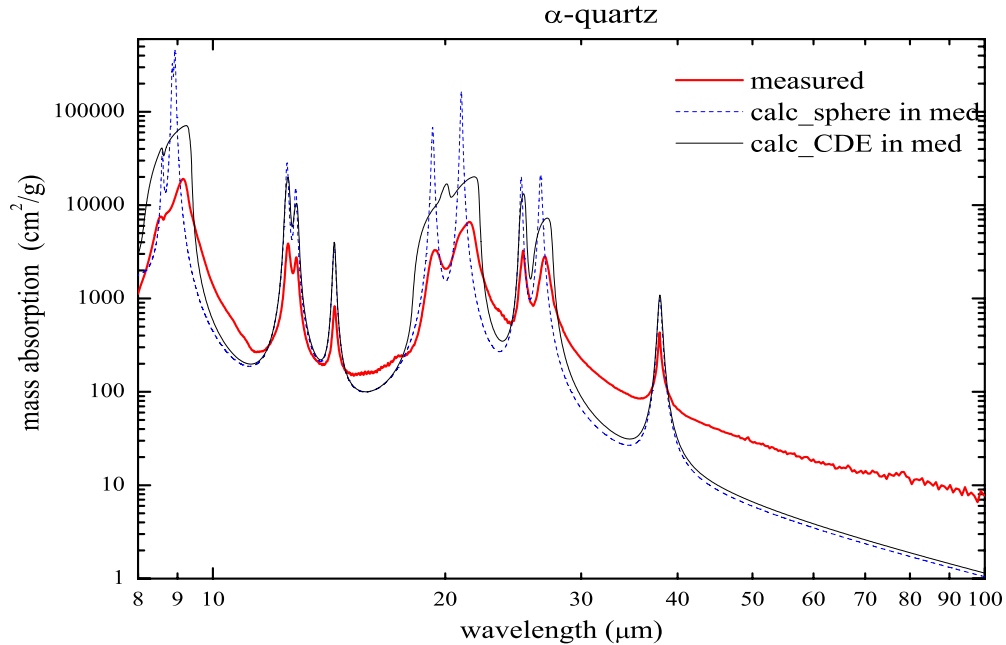


**Figure 4.** Measured IR spectra of  $\alpha$ -quartz particles in KBr and PE (thick red line) compared with calculated spectra in KBr and PE of continuously distributed ellipsoids (CDEs) and spheres (thin black and blue dotted lines, respectively) obtained using the derived optical constants by the classical dispersion theory of the measured reflectance.

(A color version of this figure is available in the online journal.)

around  $9 \mu\text{m}$  for both rays are slightly larger, and the broad peak at about  $19 \mu\text{m}$  for the extraordinary ray ( $E \parallel C$ ) has only one peak and no dip compared to the data from Spitzer & Kleinman (1961). The optical constants were derived from the measured reflectance according to the classical dispersion theory of crystals (Spitzer & Kleinman 1961). As for the peak at about  $19 \mu\text{m}$  for the extraordinary ray ( $E \parallel C$ ), our study did not require additional oscillators at  $539 \text{ cm}^{-1}$  (Spitzer & Kleinman 1961) or at  $509 \text{ cm}^{-1}$  (Wenrich & Christensen 1996) to fit the band in the spectrum. With these derived optical constants, the mass absorptions of the continuously distributed

ellipsoids (CDEs) and spheres were calculated assuming the size of the grains were within the Rayleigh limit and taking the “(2/3)–(1/3)-approximation” for the ordinary and extraordinary rays (Bohren & Huffman 1983; Sargent et al. 2006). The measured spectrum of quartz particles is more similar to that calculated for spherical grains than that calculated for CDE grains, although the measured intensities were much lower than those determined for spheres as shown in Figure 4. Our calculated spectrum for spherical grains is very similar to that calculated by Sargent et al. (2009), though our intensities were a little higher. The peak at  $78.3 \mu\text{m}$  of the measured spectra

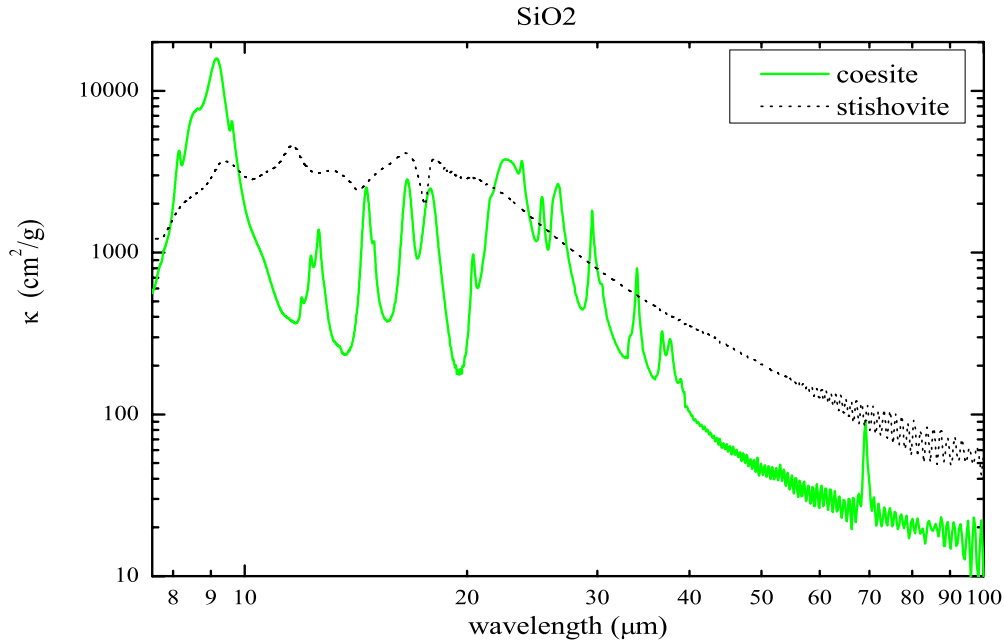


**Figure 5.** IR spectra of coesite and stishovite particles are indicated by the thick green and dotted black lines, respectively. (A color version of this figure is available in the online journal.)

of  $\alpha$ -quartz particles was very weak, and it was confirmed at  $78.1 \mu\text{m}$  with a bulk quartz ( $\alpha$ -quartz) sample (Russell & Bell 1967). This peak was not apparent from the present reflectance measurements of bulk samples.

### 3.3. Coesite

The IR spectra of coesite appeared as many sharp, fine peaks, with the main strong peaks at  $9.17$ ,  $12.3$ ,  $12.6$ ,  $14.6$ ,  $16.6$ ,  $17.8$ ,  $22.5$ ,  $23.7$ ,  $25.3$ ,  $26.5$ ,  $29.5$ ,  $33.9$ ,  $36.7$ ,  $37.6$ , and  $69.1 \mu\text{m}$  (Figure 5). These spectra are very similar to those reported by Lyon (1962), Kieffer (1979), and Williams et al. (1993).

The spectra by Lyon (1962) were measured in only limited wavelengths up to  $25 \mu\text{m}$ , and the peak at  $23.0 \mu\text{m}$  was shifted to be approximately  $0.7 \mu\text{m}$  shorter than that recorded in our data. The spectra reported by Kieffer (1979) were measured up to  $100 \mu\text{m}$ . Her reported spectra were similar to our spectra, and the weak peaks at  $11.9$ ,  $12.3$ ,  $20.4$ , and  $71.4 \mu\text{m}$  were clearly detected in the present spectra, although the peak positions shifted slightly. In particular, the peak at  $69.1 \mu\text{m}$  was certainly detected. The slightly shorter wavelength than that at  $71.4 \mu\text{m}$  was likely due to an impurity reported by Kieffer (1979). The coesite samples provided by Lyon and Kieffer were naturally shocked coesite from shocked Coconino sandstone of Meteor Crater, Arizona, and included a small amount of other minerals, which appeared at  $10.4$ ,  $11.4$ , and  $22.8 \mu\text{m}$ . For the synthetic sample, Williams et al. (1993) measured the IR spectra in the mid-IR region, which is very similar to the new data presented here.

The peak at  $69.1 \mu\text{m}$  detected first for the present coesite sample is very similar to that of forsterite but it is significantly sharper.

### 3.4. Stishovite

Stishovite is a high-density form of  $\text{SiO}_2$  with a Rutile structure and silicon in octahedral coordination  $\text{SiO}_6$ . The synthesized stishovite showed a strong resistance to grinding into fine particles. Its hardness is approximately 9.5, which is harder than

alumina. In fact, some of the present synthesized particles were contaminated with alumina particles after grinding with an alumina mortar; the smoothed surface of the alumina mortar was also damaged. The stishovite used here was ground and further mixed with KBr and PE powder in a tungsten carbide (WC) mortar. The spectra of stishovite powder showed peaks at  $9.40$ ,  $11.6$ ,  $13.1$ ,  $16.5$ ,  $18.0$ , and  $20.2 \mu\text{m}$  (Figure 5). Numerous measured spectra were previously reported by many researchers (Lyon 1962; Kieffer 1979; Spektor et al. 2011; Williams & Jeanloz 1988; Williams et al. 1993; Hofmeister et al. 1990; von Czarnowski & Hübner 1987) and were notoriously variable; that is, crystal structure is not always consistent, which gives rise to the observed variations. The natural stishovite samples were recovered by HF acid treatment from shocked Coconino sandstone of Meteor, Arizona, and were ground very finely ( $d < 100 \text{ nm}$ ); these samples likely contained impurities of minerals not soluble in HF or  $\text{HNO}_3$  (Lyon 1962; Kieffer 1979; von Czarnowski & Hübner 1987). The peaks at mid-IR wavelength reported by Lyon and by Kieffer were very similar; however, neither the peaks at  $10.5$ ,  $13.7$ ,  $14.9$ , and  $15.9 \mu\text{m}$  nor those at  $30.3$ ,  $35.1$ , and  $45.5 \mu\text{m}$  reported by Kieffer appear in our data. The IR spectra of pure synthetic stishovite were measured by Hofmeister et al. (1990), Williams & Jeanloz (1988), Williams et al. (1993), and Mohanty et al. (2009). The spectra reported by Mohanty et al. (2009) were similar to those in our data except for the peak at  $13.1 \mu\text{m}$ , which did not appear in their sample. However, their peaks at  $9.4 \mu\text{m}$  and  $20.1 \mu\text{m}$  were very weak compared with those recorded in our data. Our spectra of stishovite is very similar to the results reported by Williams & Jeanloz (1988), in which the pressure was increased to  $38.9 \text{ GPa}$  at room temperature (RT). These stishovite samples were synthesized at high pressure with controlled temperature and time durations, including  $95 \text{ kbar}$  ( $=9.5 \text{ GPa}$ ) and  $1373 \text{ K}$  (duration is unknown) by Hofmeister et al. (1990), at high pressure (up to  $46.7 \text{ GPa}$ ) and  $300 \text{ K}$  (duration time is unknown) by Williams & Jeanloz (1988) and Williams et al. (1993), and at  $12 \text{ GPa}$  and  $673 \text{ K}$  for  $5 \text{ min}$  by Mohanty et al. (2009). Our stishovite samples were compressed at  $12 \text{ GPa}$  and  $1473 \text{ K}$  for  $1 \text{ hr}$ , where a

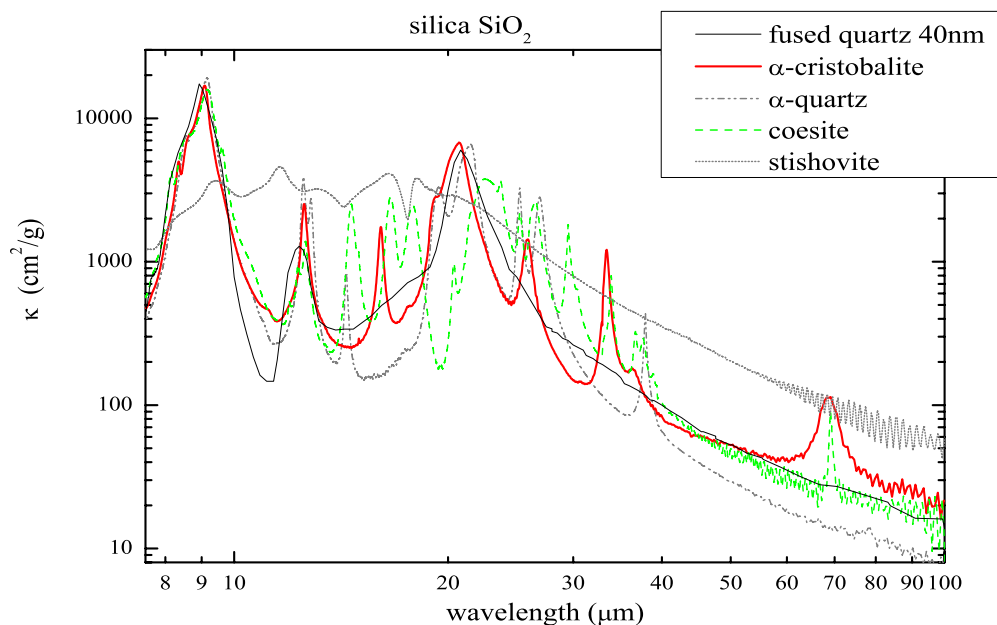


**Figure 6.** IR spectra of silica particles for the 40 nm samples of fused quartz (thin black line),  $\alpha$ -quartz (dashed-dotted gray line),  $\alpha$ -cristobalite (thick red line), coesite (dotted green line), and stishovite (broken gray line).

(A color version of this figure is available in the online journal.)

**Table 3**  
Peak Positions (in  $\mu\text{m}$ ) of the IR Spectra of the Present Samples; 40 nm Fused Quartz, and  $\alpha$ -Cristobalite Formed after Annealing the 40 nm Fused Quartz Samples at 1773 K for 3 days

$\alpha$ -Quartz	Fused Quartz	$\alpha$ -Cristobalite	Coesite	Stishovite
7.14	8.93	S	8.35	8.16
8.56	12.3	S	9.09	8.52
9.15	S	20.8	S	9.17
12.5	S	16.1	S	9.61
12.8		17.5	12.0	18.0
14.4		19.0	12.3	S
19.4		20.7	S	12.6
21.5	S	25.9	S	14.6
25.2	S	33.5	S	15.0
26.9	S	36.3	S	16.6
37.9	S	69.1	S	17.8
78.3			20.4	
			22.5	S
			23.7	S
			25.3	S
			26.5	S
			29.5	S
			30.3	
			33.2	
			33.9	S
			36.7	S
			37.6	S
			38.9	
			69.1	S

**Note.** S denotes a strong peak.

stishovite sample can be stably synthesized from phase diagram as shown in Figure 1.

### 3.5. All Samples

The spectra of all samples are compared in Figure 6. The peak positions of the present samples are listed in Table 3. The strength and peak position of the 9  $\mu\text{m}$  band were very similar for all samples except stishovite. However, many sharp peaks appeared in different bands for coesite and quartz. In the far-IR

region at approximately 69  $\mu\text{m}$ , a strong and broad band appeared for cristobalite, and a strong and sharp peak appeared for coesite.

### 3.6. Spectra at Low Temperatures Compared with Those of Forsterite

The spectra of  $\alpha$ -cristobalite and coesite showed similar bands at 16, 33, and 69  $\mu\text{m}$  to those of forsterite, as shown in Figure 7. The mineral forsterite is a significant component in circumstellar

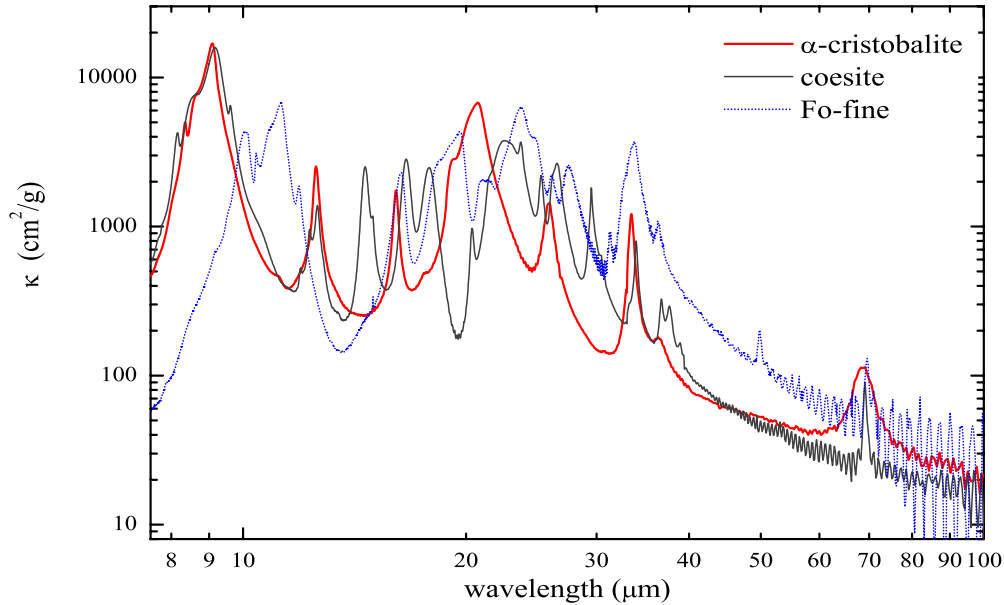


**Figure 7.** IR spectra of  $\alpha$ -cristobalite (thick red line) and coesite (thin black line) compared with that of forsterite (dotted blue line). (A color version of this figure is available in the online journal.)

dust and is ascertained by the peak positions of the observed IR spectra. Annealing magnesium silicate smokes transformed to crystalline forsterite and tridymite or cristobalite (Fabian et al. 2000; Sargent et al. 2009). If amorphous magnesium silicates grains were being heated by the central star, it may be possible that forsterite and  $\alpha$ -cristobalite grains coexist around circumstellar. To discriminate between the samples here ( $\alpha$ -cristobalite and coesite) and forsterite, the spectra of coesite and  $\alpha$ -cristobalite were measured at low temperatures from RT to 8 K (Figure 8), and the peak positions of  $\alpha$ -cristobalite and coesite were compared with those of forsterite (Figures 9 and 10), where the spectra show for above  $15 \mu\text{m}$  region as the spectra do not vary much below  $15 \mu\text{m}$  region. Most peak positions of each band shifted to shorter wavelengths and became sharper as the samples cooled from RT to 8 K; however, several peak positions shifted to longer wavelengths. In the case of  $\alpha$ -cristobalite, the peak positions of the 33 and  $36 \mu\text{m}$  bands shifted to longer wavelengths as the temperature decreased. In the case of coesite, the peak positions of the 34, 38, 39, and  $69 \mu\text{m}$  bands shifted to longer wavelengths with decreasing temperature. The differences among  $\alpha$ -cristobalite, coesite, and forsterite are clear for the  $16 \mu\text{m}$  band, as indicated by their distinguished peak positions. For the  $33 \mu\text{m}$  band, the peaks of  $\alpha$ -cristobalite and coesite were sharper than these of forsterite. For the  $69 \mu\text{m}$  band, as shown in Figures 10 and 11, the band of  $\alpha$ -cristobalite was very broad when shown in the full width at half-maximum (FWHM), and its peak position differed significantly from that of forsterite. Meaning peak positions shifted largely to shorter wavelengths as temperature decreased. Although the peak position was the same at 200 K, the band for coesite was sharper and shifted to a longer wavelength than that of forsterite at a lower temperature.

#### 4. ASTROPHYSICAL IMPLICATIONS

##### 4.1. Silica Polymorphs in Enstatite Chondrites and Lunar Meteorites

Crystalline silica ( $\text{SiO}_2$ ) grains have been identified in debris disk stars. The crystalline silica was proposed to originate as

the remnant material from the surface crust of large rocky planetesimals due to large hypervelocity impacts (Rhee et al. 2008; Lisse et al. 2009; Melis et al. 2010; Fujiwara et al. 2012b) or as a result of annealing the amorphous silica (or extremely silica-rich silicates; Sargent et al. 2009). As for the latter case, annealing amorphous magnesium silicates transformed to forsterite, tridymite, and  $\alpha$ -cristobalite or enstatite (E), according to the grain size and the kind of amorphous material (smoke or glass; Fabian et al. 2000). On the other hand, shocked E grains in meteorites are known to have formed silica polymorph inclusions (Kimura et al. 2005); the polymorphs of silica in E chondrites included quartz, tridymite, cristobalite, and silica glass, and these silica phases were crystallized from the chondrule melt. These polymorphs reflect the physical conditions of formation. Kimura et al. compared these detected silica with the phase diagram of silica and estimated the conditions of formation to glean significant information about the primary and secondary thermal processes for E chondrites. A short duration of shock-induced high-pressure conditions by small impactors may explain the occurrence of low-pressure silica polymorphs in heavily shocked E chondrites. Some E chondritic material bearing tridymite and cristobalite cooled rapidly, possibly near the surface of their parent bodies, allowing the preservation of tridymite and cristobalite. Other materials cooled slowly, at depth in the parent body, from metamorphic or crystallization temperature, allowing formation of quartz (Kimura et al. 2005). Various silica members detected in E chondrites were produced with a complicated thermal history.

Although Kimura et al. (2005) did not find high-pressure polymorphs such as coesite or stishovite in the E chondrite samples, Weisberg et al. (2006) found clusters of coesite and coesite mixed with quartz in the matrix of the Gujba CB (Bencubbin-like) chondrites, suggesting heterogeneous distribution of pressures due to shock. Further, Ohtani et al. (2011) found several silica polymorphs such as coesite, stishovite, and quartz in amorphous silica grains in the Asuka-991757 lunar meteorite, which experienced an equilibrium shock pressure of at least 8–30 GPa. This result suggests that high-pressure impact metamorphism and formation of high-pressure minerals are common

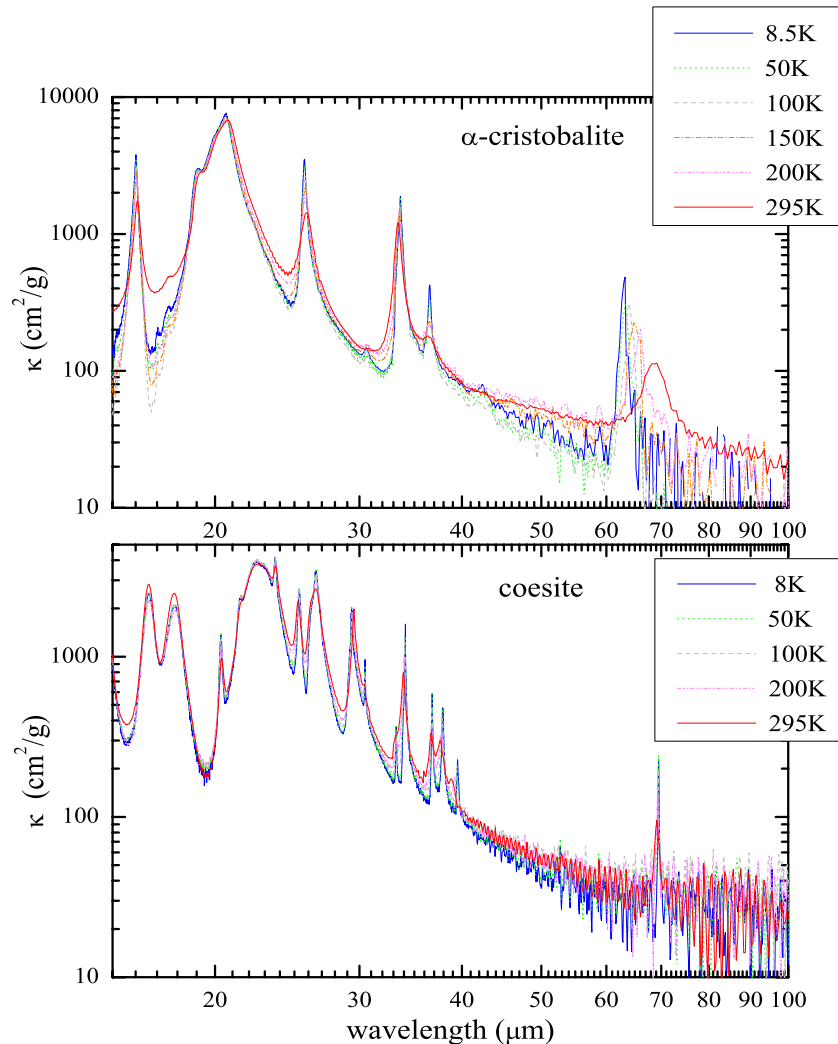


**Figure 8.** Spectra of  $\alpha$ -cristobalite (upper) and coesite (lower) cooled at low temperatures, including RT (thick red line), 200 K (dotted-dotted-dashed pink line), 150 K (dotted-dashed orange line), 100 K (dashed gray line), 50 K (dotted green line), and 8 K (thin blue line).

(A color version of this figure is available in the online journal.)

phenomena in brecciated lunar surfaces altered by heavy meteoritic bombardment.

In ordinary chondrites, it is notable that such silicas as tridymite, cristobalite, quartz, and glass are identified—though these are rare cases: these silica were formed in the solar nebula by fractional condensation, reheating to temperatures above 1140 K probably during the chondrule forming process, followed by rapid cooling (Hezel et al. 2006).

In these materials of chondrites and lunar samples, detections of silica phase may depend on the composition of the bulk and on limited area (on the scale of millimeters or less). On the other hand, glass with embedded metal and sulfides (GEMS) grains have been proposed to be one of the most primitive materials in the solar system (though their origins are controversial); GEMS grains were originally interstellar dust particles (Bradley & Dai 2004) or formed by gas condensation in the early solar nebula (Keller & Messenger 2011). The chemical compositions of GEMS particles are almost similar to the solar abundance of the elements, but the mean composition is more  $\text{SiO}_2$ -rich than solar abundance, where silicate portions are more  $\text{SiO}_2$ -rich than pyroxene (Matsuno et al. 2012). GEMS grains must have been an important starting component of other primitive meteoritic materials and likely had a profound influence on the

earliest stages of their evolution (Keller & Messenger 2011; Matsuno et al. 2012). In order to detect silica grains around debris disks, there must be a considerable amount silica grains. To create silica minerals, either annealing amorphous silicate such as GEMS or primitive meteoritic materials and/or large hypervelocity impacts as mentioned above are required.

#### 4.2. Detection of Silica in Debris Disks

Around TTSS, annealed silica (cristobalite and/or tridymite) is apparent from mid-IR observations, in which the annealing of amorphous silica near TTSS was first proposed (Sargent et al. 2009). In this case, the important point is to determine whether the temperature of the circumstellar disk can be raised to above 1673–1773 K instead of 1220 K by the heating up of the central star. Otherwise, an additional process such as heating by collision must be introduced to explain the existing peak of the  $16 \mu\text{m}$  band of  $\alpha$ -cristobalite.

By annealing amorphous magnesium silicates, they change to forsterite, tridymite,  $\alpha$ -cristobalite, and enstatite (Fabian et al. 2000). From these results, forsterite and  $\alpha$ -cristobalite may exist together around disks. For evidence of existing  $\alpha$ -cristobalite, the broad and strong band at approximately  $69\text{--}62 \mu\text{m}$  could be

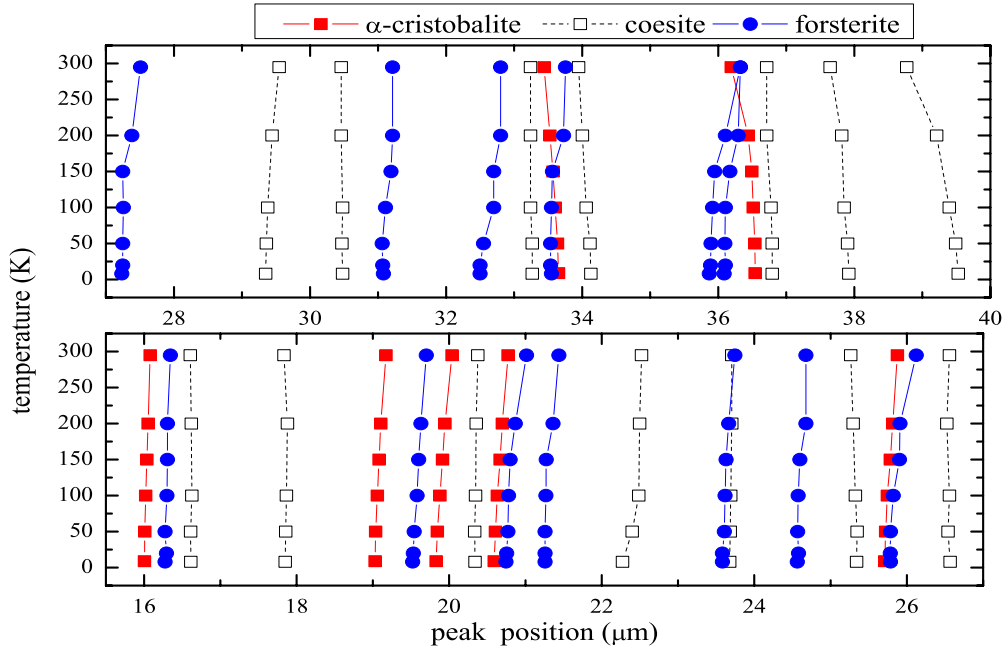


**Figure 9.** Temperature dependence of the peak positions for  $\alpha$ -cristobalite, coesite, and forsterite. (A color version of this figure is available in the online journal.)

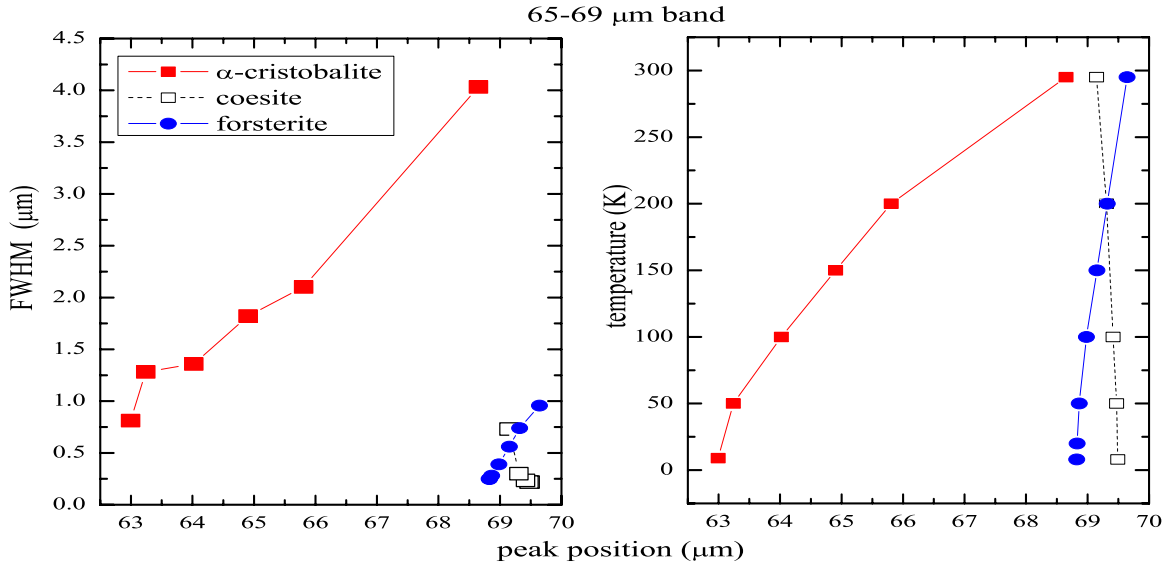


**Figure 10.** Peak position dependence at FWHM of the  $69\ \mu\text{m}$  band (left) and of the temperature (right) of  $\alpha$ -cristobalite and coesite compared with those of forsterite. (A color version of this figure is available in the online journal.)

detected through more detailed observations in far-IR regions, as shown in Figures 8 and 11. If mineral dust of coesite and  $\alpha$ -cristobalite could exist near debris disks after being produced by high-speed collisions among planetesimals, then this characteristic band could be detected by high-resolution observations in the  $60\text{--}70\ \mu\text{m}$  regions, although the presence of cold dust has not been confirmed around the outer region disk of the HD 15407 (Fujiwara et al. 2012a). This band is highly sensitive to the surrounding temperature, and this peak clearly appeared below approximately 540 K (Zhang & Scott 2007). Regarding the observed spectra of the debris disks of HD 15407 (Fujiwara et al. 2012b), the silica ( $\alpha$ -cristobalite and fused quartz) and  $1.5\ \mu\text{m}$  sized amorphous pyroxene fit well to the observed peaks at the 9, 16, and  $20\text{--}22\ \mu\text{m}$  bands, where it

is assumed that  $T_{\text{silica}} = T_{\text{silicate}} = 615\ \text{K}$ . The broadness of the peaks may be explained by an increase in temperature from RT to  $\sim 540\ \text{K}$ , where the  $16\ \mu\text{m}$  band broadens (Zhang & Scott 2007; Swainson et al. 2003; Finnie et al. 1994), rather than an increase in the size of the dust particles. Detection of the  $16\ \mu\text{m}$  peak depends on the temperature near the circumstellar disk, where  $\alpha$ -cristobalite clearly shows a peak at  $16\ \mu\text{m}$  at a temperature below  $\sim 540\ \text{K}$ . Thus, detection of the  $16\ \mu\text{m}$  peak reveals that the ambient temperature may be under  $\sim 540\ \text{K}$ . As the temperature increases to about 540 K, each peak of  $\alpha$ -cristobalite broadens. If the temperature exceeds the transition temperature of approximately  $500\text{--}550\ \text{K}$ ,  $\alpha$ -cristobalite alters to  $\beta$ -cristobalite, as shown in Table 1, and the peaks at 16, 26, 33, and  $69\ \mu\text{m}$  disappear (Zhang & Scott 2007; Swainson

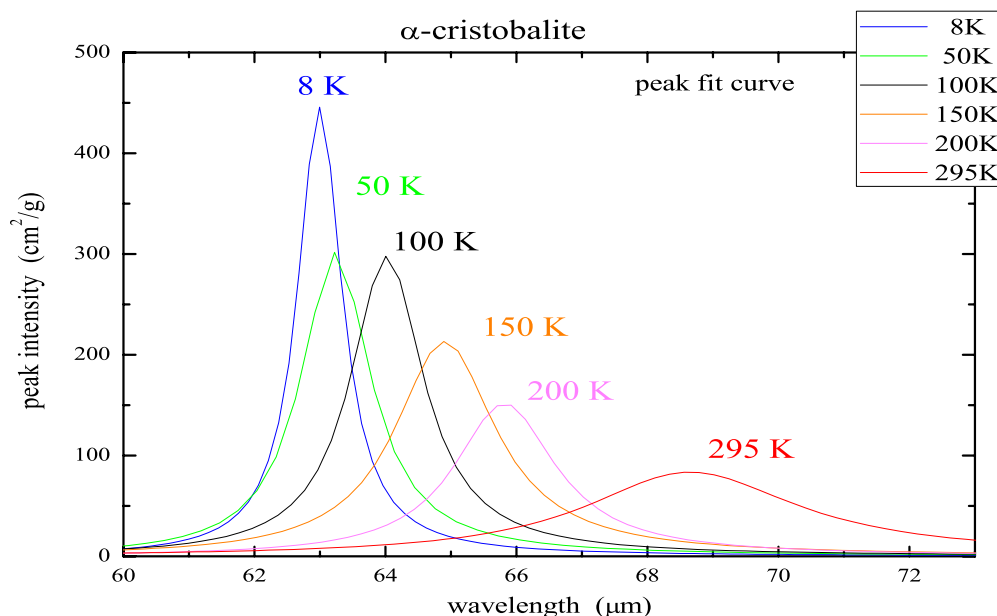


**Figure 11.** The 69  $\mu\text{m}$  band of  $\alpha$ -cristobalite showing a shift to short wavelengths as the temperature decreases. (A color version of this figure is available in the online journal.)

et al. 2003; Finnie et al. 1994). The 26, 33, and 69  $\mu\text{m}$  peaks may appear or disappear with the grain temperature like the 16  $\mu\text{m}$  peak. The 16  $\mu\text{m}$  peak disappears after heating above  $\sim 540$  K and then reappears after cooling below  $\sim 540$  K, and the transition is completely reversible and thermal hysteresis displays (Finnie et al. 1994). The observations of these peaks (peak position and FWHM) may become a diagnostic for characteristic grain temperatures like the 69  $\mu\text{m}$  band of forsterite.

As for detection of quartz grains around circumstellar disks, characteristic peaks appear at about 9.15, 12.5, and 37.9  $\mu\text{m}$  in the *Spitzer*-IRS spectrum of IS Tau. Honda et al. (2003) detected quartz at about 9.2 and 12.5  $\mu\text{m}$  in the 10  $\mu\text{m}$  spectrum of T Tauri HEN 3-600A. Furthermore, Watson et al. (2009) also detected  $\alpha$ -quartz grains at around the 9.3 and 12.5  $\mu\text{m}$  features in *Spitzer*-IRS spectrum of IS Tau. As Hezel et al. (2006) pointed out, the discovery of silica beside olivine and pyroxene in protosolar disks around the low-mass TTS HEN 3-600A (Honda et al. 2003) indicated that evaporation, recondensation, and mixing of chondrule melts may well have occurred. If observations could be made well for longer wavelengths up to 40  $\mu\text{m}$ , the characteristic peak at 37.9  $\mu\text{m}$  of  $\alpha$ -quartz grains may be detected as a strong and sharp band.

The stishovite samples were synthesized under the Visiting Researcher's Program of the Institute for Study of the Earth's Interior, Okayama University. We thank Professor Yoneda and Professor Yamazaki for their help in preparing the samples. We thank Dr. H. Isobe (Kumamoto University) for providing commercial cristobalite samples. A.T. was supported by a grant-in-aid of the Japan Ministry of Education, Culture, Sports, Science, and Technology (19104012). We would like to express thanks to the referee, Angela Speck, for her helpful comments that greatly improved this paper.

## REFERENCES

Bates, J. B. 1972, *JChPh*, **57**, 4042  
 Begemann, B., Dorschner, J., Henning, T., et al. 1997, *ApJ*, **476**, 199

Bohren, C. F., & Huffman, D. R. 1983, *Absorption and Scattering of Light by Small Particles* (New York: Wiley)  
 Bradley, J. P., & Dai, Z. R. 2004, *ApJ*, **617**, 650  
 Deer, W. A., Howie, R. A., & Zussman, J. 1999, *An Introduction to the Rock Forming Minerals* (2nd ed.; London: Longman)  
 Fabian, D., Jäger, C., Henning, T., et al. 2000, *A&A*, **364**, 282  
 Finnie, K. S., Thompson, J. G., & Withers, R. L. 1994, *JPCS*, **55**, 23  
 Fujiwara, H., Onaka, T., Takita, S., et al. 2012a, *ApJL*, **759**, L18  
 Fujiwara, H., Onaka, T., Yamashita, T., et al. 2012b, *ApJL*, **749**, L29  
 Hezel, D. C., Palme, H., Nasadala, L., & Brenker, F. E. 2006, *GeCoA*, **70**, 1548  
 Hofmeister, A. M., Xu, J., & Akimoto, S. 1990, *AmMin*, **75**, 951  
 Honda, M., Kataza, H., Okamoto, Y., et al. 2003, *ApJL*, **585**, L59  
 Keller, L. P., & Messenger, S. 2011, *GeCoA*, **75**, 5336  
 Kemper, F., Vriend, W. J., & Tielens, A. G. G. M. 2004, *ApJ*, **609**, 826  
 Kieffer, S. W. 1979, *RvGSP*, **17**, 20  
 Kimura, M., Weisberg, M. K., Lin, Y., et al. 2005, *M&PS*, **40**, 855  
 Klein, C., & Hurlbut, C. S. 1993, *Manual of Mineralogy* (21st ed.; New York: Wiley)  
 Koike, C., Mutschke, H., Suto, H., et al. 2006, *A&A*, **449**, 583  
 Koike, C., & Shibai, H. 1994, *MNRAS*, **269**, 1011  
 Lisse, C. M., Chen, C. H., Wyatt, M. C., et al. 2009, *ApJ*, **701**, 2019  
 Luo, S., Swadener, J. G., Ma, C., & Tschauer, O. 2007, *PhysB*, **399**, 138  
 Lyon, R. J. P. 1962, *Natur*, **196**, 267  
 Malfait, K., Waelkens, C., Waters, L. B. F. M., et al. 1998, *A&A*, **332**, L25  
 Matsuno, J., Tshuchiyama, A., Koike, C., et al. 2012, *ApJ*, **753**, 141  
 Melis, C., Zuckerman, B., Rhee, J., & Song, I. 2010, *ApJL*, **717**, L57  
 Meng, H. Y. A., Rieke, G. H., Su, K. Y., et al. 2012, *ApJL*, **751**, L17  
 Mohanty, P., Li, D., Liu, T., et al. 2009, *JChS*, **131**, 2764  
 Molster, F. J., Waters, L. B. F. M., & Tielens, A. G. G. M. 2002, *A&A*, **382**, 222  
 Nishiyama, N., Seike, S., Hamaguchi, T., et al. 2012, *Scripta Materialia*, **67**, 955  
 Ocaña, M., Fornes, V., Garcia-Ramos, J. V., & Serna, C. J. 1987, *PCM*, **14**, 527  
 Ohtani, E., Ozawa, S., Miyahara, M., et al. 2011, *PNAS*, **108**, 463  
 Olofsson, J., Juhász, A., Henning, Th., et al. 2012, *A&A*, **542**, 90  
 Plendl, J. N., Mansur, L. C., Hadni, A., et al. 1967, *JPCS*, **28**, 1589  
 Rhee, J., Song, I., & Zuckerman, B. 2008, *ApJ*, **675**, 7777  
 Russell, E. E., & Bell, E. E. 1967, *JOSA*, **57**, 341  
 Sargent, B., Forrest, W., Tayrien, C., et al. 2009, *ApJ*, **690**, 1193  
 Sargent, B., Forrest, W. J., D'Alessio, P., et al. 2006, *ApJ*, **645**, 395  
 Šimon, I., & McMahon, H. O. 1953, *JChPh*, **21**, 23  
 Speck, A. K. 1998, PhD thesis, Univ. College London  
 Speck, A. K., Barlow, M. J., Sylvester, R. J., & Hofmeister, A. M. 2000, *A&AS*, **146**, 437  
 Speck, A. K., Whittington, A. G., & Hofmeister, A. M. 2011, *ApJ*, **740**, 93  
 Spektor, K., Nylen, J., Stoyanov, E., et al. 2011, *PNAS*, **108**, 20918  
 Spitzer, W. G., & Kleinman, D. A. 1961, *PhRv*, **121**, 1324  
 Swainson, I. P., Dove, M. T., & Palmer, D. C. 2003, *PCM*, **30**, 353  
 Swamy, V., & Saxena, S. K. 1994, *JGR*, **99**, 11787

Technical Reformance Specs 2012, in Abrasion Resistance, stonessource.com  
von Czarnowski, A., & Hübner, K. 1987, PSSBR, [142](#), [K91](#)  
Watson, D. M., Leisenring, J. M., Furlan, E., et al. 2009, [ApJS](#), [180](#), [84](#)  
Weisberg, M. K., Kimura, M., Suzuki, A., et al. 2006, in 37th Lunar and Planetary  
Science Conf., ed. S. Mackwell & E. Stansbery (Houston, TX: Lunar and  
Planetary Institute), [1788](#)

Wenrich, M. L., & Christensen, P. R. 1996, [JGR](#), [101](#), [15921](#)  
Williams, Q., Hemley, R. J., Kruger, M. B., & Jeanloz, R. 1993, [JGR](#), [98](#),  
[22157](#)  
Williams, Q., & Jeanloz, R. 1988, [Sci](#), [239](#), [4842](#)  
Yahagi, Y., Yagi, T., Yamawaki, H., & Aoki, K. 1994, [SSCom](#), [89](#), [945](#)  
Zhang, M., & Scott, J. F. 2007, [JPCM](#), [19](#), [275201](#)